Discrete & Computational Geometry
https://doi.org/10.1007/s00454-025-00756-z

On the Long-Range Order of the Spectre Tilings

Michael Baake[1] · **Franz Gähler**[1] · **Jan Mazáč**[1] · **Lorenzo Sadun**[2]

Received: 25 November 2024 / Revised: 12 June 2025 / Accepted: 13 June 2025
© The Author(s) 2025

Abstract
The Spectre is an aperiodic monotile for the Euclidean plane that is truly chiral in the sense that it tiles the plane without any need for a reflected tile. The topological and dynamical properties of the Spectre tilings are very similar to those of the Hat tilings. Specifically, the Spectre sits within a complex 2-dimensional family of tilings, most of which involve two shapes rather than one. All tilings in the family give topologically conjugate dynamics, up to an overall rescaling and rotation. They all have pure-point dynamical spectrum with continuous eigenfunctions and may be obtained from a $4 : 2$ dimensional cut-and-project scheme with regular windows of Rauzy fractal type. The diffraction measure of any Spectre tiling is pure-point as well. For fixed scale and orientation, varying the shapes is MLD equivalent to merely varying the projection direction. These properties all follow from the first Čech cohomology being as small as it possibly could be, leaving no room for shape changes that alter the dynamics.

Keywords Tiling cohomology · Dynamical spectra · Model sets · Deformations · Monotile

Mathematics Subject Classification 52C20 · 37D40 · 55N05 · 52C23

Editor in Charge: Kenneth Clarkson

Michael Baake
mbaake@math.uni-bielefeld.de

Franz Gähler
gaehler@math.uni-bielefeld.de

Jan Mazáč
jmazac@math.uni-bielefeld.de

Lorenzo Sadun
sadun@math.utexas.edu

[1] Fakultät für Mathematik, Universität Bielefeld, Postfach 100131, 33501 Bielefeld, Germany

[2] Department of Mathematics, University of Texas, 2515 Speedway, PMA 8.100, Austin, TX 78712, USA

Published online: 01 September 2025

Content courtesy of Springer Nature, terms of use apply. Rights reserved.

1 Introduction and Previous Results

In 2023, Smith et al. [20] surprised the world with their discovery of an aperiodic monotile, which is simply connected in contrast to the Socolar–Taylor monotile [23]. The *Hat* is a non-convex polykite with 14 edges (two of which are back to back and look like a double-length edge) and no reflection symmetry. You can tile the Euclidean plane with isometric copies of the Hat, but the resulting tilings cannot have any translational symmetry. All such tilings require both rotated Hat tiles and rotated versions of the reflected Hat, often called the *anti-Hat*; see the figures in [20] for an illustration of the tiles and a finite patch of the tiling.

A mere two months after the discovery of the Hat, the same author team constructed a chiral (reflection-free) analogue, now known as the *Spectre* [21], by modifying one of the tiles in the Hat family. As with the Hat, there are 12 Spectre tiles up to translation. The resulting tilings are non-periodic and have statistical 6-fold rotational symmetry, meaning that each patch occurs in all six orientations with equal frequencies. The 12 tiles can be divided into two classes. Instead of being related by reflection, the two classes are related by rotation by 30°. That is, one only needs a single tile and rotations of that tile by multiples of 30° to tile the plane, with all of the resulting tilings being non-periodic.

Spectre tilings do not have statistical 12-fold symmetry. Instead, one group of 6 tiles occurs with much greater frequency than the other. This means that there are actually two local indistinguishability classes (LI classes, see [7, Def. 5.5]) obtained from a fixed set of 12 Spectre tiles, each of which is a 30° rotation of the other.

In this paper, we study the dynamics and topology of the Spectre tilings. As with the Hat tilings (compare [5]), we will show that there is a complex 4-dimensional family of Spectre-like tilings, all of which have topologically conjugate translational dynamics, up to linear transformation. Within this 4-dimensional family, there is a 2-dimensional subfamily (including the original Spectre) that maintains 6-fold statistical symmetry. These all have topologically conjugate dynamics, up to rotation and scale. We only need to understand the dynamics of one tiling in this family to understand all of them. A crucial method for establishing all this is the Čech cohomology of the induced tiling spaces, see [19] for a general introduction and [20] for the analogous treatment of the Hat tilings, in conjunction with the classification of shape changes from [9].

Within the 2-dimensional family, there is a special tiling that we call *CASPr* (for Cut-And-Symmetrically-Project). This tiling admits a geometric substitution (an inflation rule that defines a self-similar tiling). Many techniques exist for studying such self-similar tilings. Using a generalization of Solomyak's *Overlap Algorithm* [3, 24], we verify that the CASPr tiling has pure-point dynamical spectrum. In addition, we use the known equivalence of pure-point diffraction and dynamical spectra [8] to show the same result via the cut-and-project method. This also implies that it can be obtained via a cut-and-project scheme, for which we compute the lattice and the window. More precisely, we select a Delone set that is *mutually locally derivable* (MLD) from the CASPr tiling and admits such a description; see [7, Sec. 5.2] for background on this local version of topological conjugacy. All other 6-fold symmetric tilings in the Spectre tiling family, including the original Spectre tiling, are MLD to modified Delone sets that are obtained from essentially the same cut-and-project scheme. One uses the same

Content courtesy of Springer Nature, terms of use apply. Rights reserved.

total space and the same window to generate the different point patterns in $\mathbb{R}^4$, only with different projections from $\mathbb{R}^4$ to $\mathbb{R}^2$—a situation that is once again analogous to that of the Hat versus the CAP tiling [5].

The structure of the paper is as follows. In Sect. 2, we review the geometry of the Hat and Spectre tiles and explain how to build a complex 2-dimensional family of Spectre-like tilings with 6-fold statistical symmetry. In Sect. 3, we then compute the Čech cohomology of each space of Spectre tilings. This calculation shows that all shape deformations of the Spectre (including those that break rotational symmetry) are topologically conjugate to the Spectre up to linear transformation, and that our 2-dimensional family that respects rotational symmetry is conjugate to the Spectre up to rotation and scale.

In Sect. 4, we construct the CASPr tiling and compute its return module. In Section 5, we construct the cut-and-project scheme that yields the CASPr tiling and show that it has pure-point spectrum. In Sect. 6, we show that our entire 2-dimensional family of Spectre-like tilings are MLD to Delone sets that can be obtained by merely rescaling, rotating, and varying the projection direction of the CASPr tiling.

2 Geometry of Hat and Spectre Tiles

As seen from the figures in [20], a tile in the Hat family is a polygon with 8 edges of length a and 6 edges of length b. We identify $\mathbb{R}^2$ with $\mathbb{C}$ with the real axis being *vertical*; this unusual convention will prove useful when we consider the Spectre. The basic Hat tile has 8 edges whose displacements are a times powers of $\xi = e^{2\pi i/6} = (1+i\sqrt{3})/2$ and 6 edges whose displacements are ib times powers of ξ. We refer to this shape as Tile(a, b). However, there is no reason why a and b have to be real. We can consider shapes where a and b are complex numbers, with the displacements along edges being a or ib times powers of ξ. This gives a family of tile shapes of complex dimension 2 (real dimension 4). Notable elements of this family include Tile$(0, 1)$ (the Chevron), Tile$(1, \sqrt{3})$ (the Hat), Tile$(1, 1)$ (the Spectre), Tile$(\sqrt{3}, 1)$ (the Turtle) and Tile$(1, 0)$ (the Comet). For the Turtle, an alternate proof of aperiodicity was presented in [1].

A Hat-like tiling is made from Tile(a, b) in 6 orientations and the reflection of Tile$(\bar{a}, \bar{b})$ in 6 orientations. (We define our standard reflection m to be horizontal: $m(x, y) = (-x, y)$. With our identification of $\mathbb{R}^2$ with $\mathbb{C}$, this is equivalent to complex conjugation.) If a/b is real, all of the tiles are isometric and we have a monotile. However, even if a/b is complex (in which case Tile$(\bar{a}, \bar{b})$ is not isometric to Tile(a, b)), we still have a well-defined space of tilings.

A Spectre-like tiling is made from Tile(a, b) rotated by even multiples of 30° and Tile(b, a) rotated by odd multiples of 30°. For the ratio $a/b = 1$, we have only one tile type, the Spectre. A patch of such a Spectre tiling is shown in Fig. 1. If we vary the ratio a/b to $\sqrt{3}$, we get two tile types: the even Spectres become Hats and the odd Spectres become Turtles, as shown in the combinatorially equivalent patch in Fig. 2. Indeed, the proof of aperiodicity in [21] is based on analyzing a tiling by Hats and Turtles that is combinatorially equivalent to a tiling by even and odd Spectres. The version with Hats and Turtles has the advantage that the tiles are located on an underlying hexagonal lattice. For the Spectre tiling, this is not the case.

Content courtesy of Springer Nature, terms of use apply. Rights reserved.

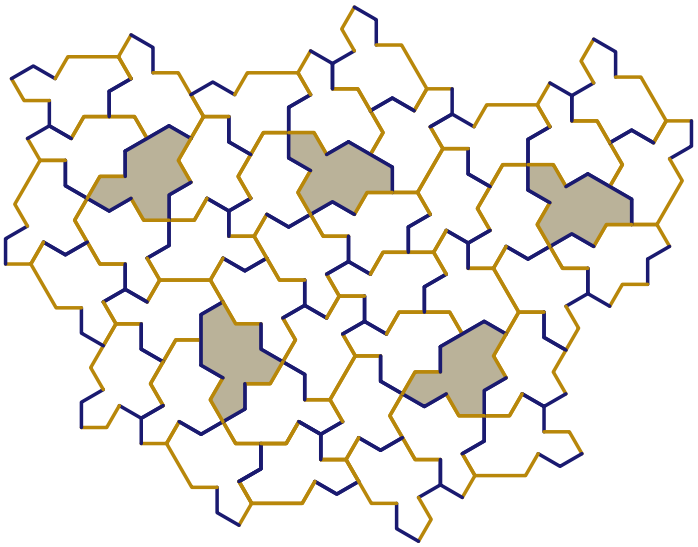

Fig. 1 Patch of a Spectre tiling. Up to rotation, there is only one tile type. Spectres in minority (odd) orientations are shaded. Edges of types a and b are distinguished by color

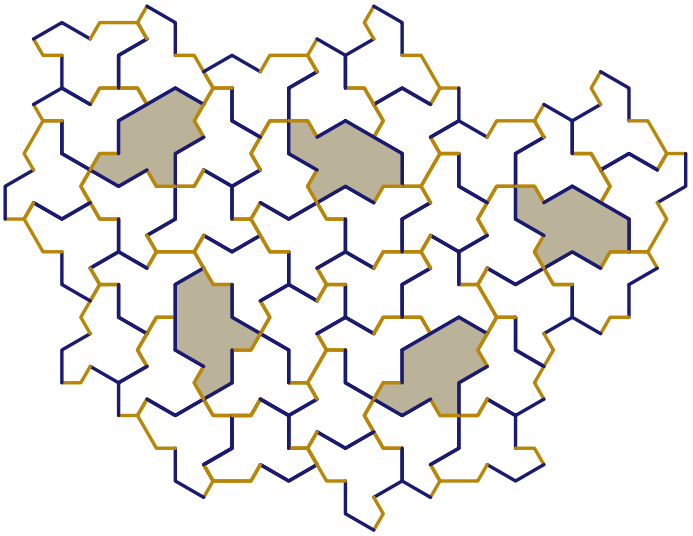

Fig. 2 A combinatorially equivalent tiling to Fig. 1, in which all even Spectres are replaced by Hats and all odd Spectres by Turtles. To achieve this, the length ratio of the two kinds of edges is changed from 1 to $\sqrt{3}$

It is immediate that the Hat–Turtle tilings (with $a/b = \sqrt{3}$) and the Spectre tilings (with $a/b = 1$) are related by a *shape change* of the tiles, maintaining the combinatorics of the tilings. Such shape changes are classified, up to local equivalence, by $\check{H}^1(\Omega, \mathbb{R}^2)$, the first Čech cohomology of the tiling space with values in $\mathbb{R}^2$, see [9], or equivalently

Content courtesy of Springer Nature, terms of use apply. Rights reserved.

by $\check{H}^1(\Omega, \mathbb{C})$, with a subgroup of $\check{H}^1(\Omega, \mathbb{C})$ parametrizing shape changes that are topological conjugacies. The calculations of Sect. 3 will imply that the translation actions of the two tiling dynamical systems are topologically conjugate.

Note that Tile(a, b) is only isometric to Tile(b, a) when $a = b$. While there is a large family of Spectre-like tilings, there is essentially only one chiral monotile, namely the actual Spectre Tile(1, 1). We note in passing that it is possible to make a periodic tiling from Tile(1, 1) and its reflection. To eliminate this possibility, the authors of [21] added edge markings to Tile(1, 1) that prevent Spectres and anti-Spectres from fitting together. If one simply defines the prototile set to include tiles but not anti-tiles, such decorations are unnecessary.

3 Substitutive Structure and Cohomology

In the Spectre tilings, as in the Hat tilings, tiles aggregate into clusters called *meta-tiles*. These meta-tiles assemble into larger clusters with the same combinatorial structure as the meta-tiles, which assemble into still larger structures, and so on. This fits well into the setting of fusion rules [11]. That is, both the Hat and the Spectre tilings are (combinatorial) substitution tilings, and so can be studied with a variety of well-established topological and dynamical tools. There are technical differences, of course, and the details are more complicated with the Spectre than with the Hat, but the overall picture is very similar.

The substitutive structure of the Spectre tiling was described in [21]. Imagine a Spectre tiling in which even Spectres outnumber odd Spectres. A combinatorially equivalent Hat–Turtle tiling would feature isolated Turtles in a sea of Hats. There is one and only one way for a Turtle to be surrounded by Hats. Combining the Turtle with a particular one of its surrounding Hats yields a shape called a *Mystic*. The corresponding tiling can then be described as a substitution involving two basic units: Mystics, and Hats that are not part of Mystics.

However, there are two major complications. The first is that the substituted Hats and Mystics are not made up of (rotated) Hats and Mystics. Instead, they are made up of (rotated and) *reflected* Hats and Mystics, also known as anti-Hats and anti-Mystics. Likewise, a substituted anti-Hat or anti-Mystic is a cluster of ordinary Hats and Mystics. However, we are interested in tilings that only involve Hats and Mystics, not anti-Hats or anti-Mystics! To go from Hats and Mystics to Hats and Mystics, we must apply the substitution twice, getting much larger clusters that are cumbersome to work with.

Put another way, we have a substitution σ that takes Hats and Mystics to anti-Hats and anti-Mystics. The reflection of this rule gives a substitution σ^* that takes anti-Hats and anti-Mystics to Hats and Mystics. The total substitution on all four kinds of tiles is given by the matrix

$$\begin{pmatrix} 0 & \sigma^* \\ \sigma & 0 \end{pmatrix},$$

Content courtesy of Springer Nature, terms of use apply. Rights reserved.

which swaps the unreflected and reflected sectors. The square of the substitution is then

$$\begin{pmatrix} \sigma^*\sigma & 0 \\ 0 & \sigma\sigma^* \end{pmatrix},$$

which preserves sectors. Since we are interested only in unreflected tiles, we need to study $\sigma^*\sigma$, which we accomplish by studying σ in a suitable way.

The second complication is that the substitution of Hats and Mystics does not *force the border* in the sense of [14]. In their proof of aperiodicity, Smith et al. [21] introduced a substitution involving nine meta-tiles. One is a substituted Mystic, denoted Γ. The other eight are distinct collared versions of the substituted Hat, denoted by Δ, Θ, Λ, Ξ, Π, Σ, Φ and Ψ. With this additional structure, the substitution does force the border, so we can apply the methods of Anderson and Putnam [2] to compute the Čech cohomology, as we now do.

These nine meta-tiles all are combinatorial hexagons that meet edge to edge. For the Hat–Turtle tiling, they are shown in [21, Fig. 4.1]. The tiling with the Hats and Turtles composed to meta-tiles is MLD to the plain Hat–Turtle tiling. The meta-tile tiling of combinatorial hexagons is then related by a shape change to a combinatorially equivalent tiling of *regular* hexagons, so that, up to MLD conjugacies, the latter is also related by a shape change to the original Spectre tiling.

There are 8 kinds of edges of the meta-tiles, labeled $\alpha, \beta, \gamma, \delta, \varepsilon, \zeta, \theta$, and η. We use them in this order for reasons that will become clear shortly. There are three kinds of vertices, labeled p, q and s. The geometric and combinatorial information is distilled in Fig. 3, showing each meta-tile as a regular hexagon with labeled edges and colored vertices.

Let r denote counterclockwise rotation by 60°. Each of the 9 displayed meta-tiles in standard orientation can be multiplied by r^m with $m \in \{0, 1, \ldots, 5\}$. The first 7 edge types are directional, so α, $r\alpha$, etc. are distinct. The reference orientation for each edge is vertical, pointing up. (Recall that this is the positive real direction in our identification of $\mathbb{R}^2$ with $\mathbb{C}$.) The small mark used in [21] to indicate the orientation of an edge has been replaced by the power of r needed to map the standard edge to the given one. The last edge type, η, is non-directional. It is invariant under rotation by 180°, and occurs only in three rotational variants. As a chain, $r^3\eta = -\eta$. The vertices p and q have 3-fold symmetry, so $r^2 p = p$ and $r^2 q = q$. The third vertex, s, does not have any rotational symmetry, so $s, rs, \ldots, r^5 s$ are distinct.

The substitution in terms of hexagons is shown in Fig. 4, adapted from [21, Fig. 5.1]. Specifically, it shows the action of σ^*, which turns reflected tiles into ordinary tiles. The nine pictures show what happens when you take the nine meta-tiles in standard orientation, reflect them (horizontally) and then substitute. We now have all prerequisites to state and prove the following result. We employ a strategy where all arguments can be checked by hand, so do not need any computer-assisted steps.

Theorem 1 *Let Ω be the orbit closure of a Spectre (or Hat–Turtle) tiling. The first complex Čech cohomology of Ω is*

$$\check{H}^1(\Omega, \mathbb{C}) = \mathbb{C}^4.$$

Content courtesy of Springer Nature, terms of use apply. Rights reserved.

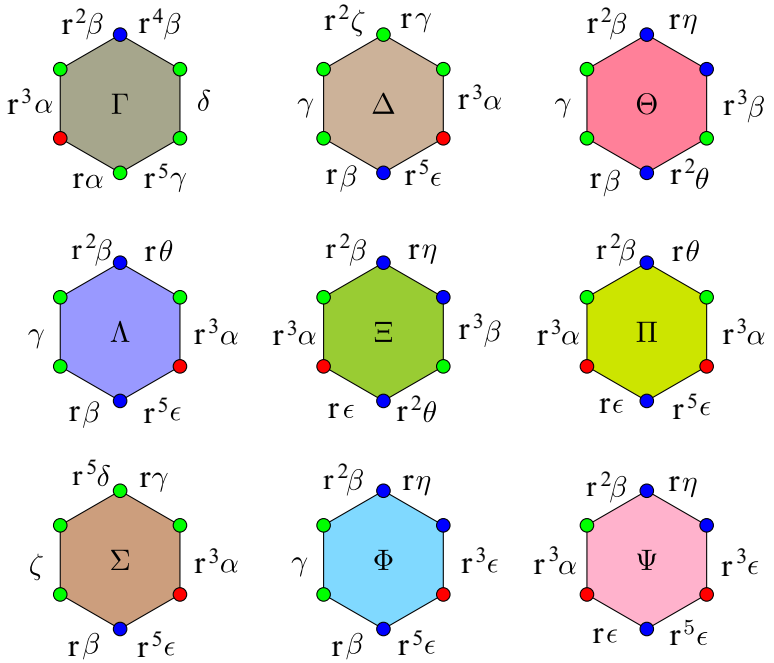

Fig. 3 The nine combinatorial hexagons (adapted from [21, Fig. 4.2]). Vertices of type p, q, and s are colored in red, blue, and green, respectively. Type and orientation of the edges are given by their labels, the power of r determining the orientation

Furthermore, this $\mathbb{C}^4$ *decomposes as a* $\mathbb{C}^2$ *from the fundamental* $r = \xi$ *representation of the cyclic group* C_6 *and a* $\mathbb{C}^2$ *from the representation* $r = \xi^5$. *The eigenvalues of the* (*squared*) *substitution on each* $\mathbb{C}^2$ *are* $4 \pm \sqrt{15}$, *each with multiplicity* 1.

The second complex Čech cohomology of Ω *is*

$$\check{H}^2(\Omega, \mathbb{C}) = \mathbb{C}^{10},$$

with a contribution $\mathbb{C}^2$ *from each* $r \in \{1, -1, \xi, \xi^5\}$ *and a single* $\mathbb{C}$ *from* $r = \xi^2$ *and* $r = \xi^4$.

Proof By the results of [2, Thms. 6.1 and 6.3], the Čech cohomology of a substitution tiling space is the direct limit of the (ordinary) cohomology of the Anderson–Putnam (AP) complex Γ_{AP} under substitution. We will first compute the cohomology of Γ_{AP} and then take the direct limit. Since we are working over the complex numbers, this is the same as the direct sum of the eigenspaces of $H^*(\Gamma_{\text{AP}}, \mathbb{C})$ under substitution with non-zero eigenvalues.

The AP complex is built from one copy of each tile type via identifying edges (and therefore vertices) where two tiles can meet. This information is already encoded in Fig. 3. Including rotations (as we must), there are 54 faces (9 shapes in 6 orientations), 45 edges (7 in 6 orientations and η in 3 orientations), and 10 vertices (p and q in 2 orientations and s in 6).

Content courtesy of Springer Nature, terms of use apply. Rights reserved.

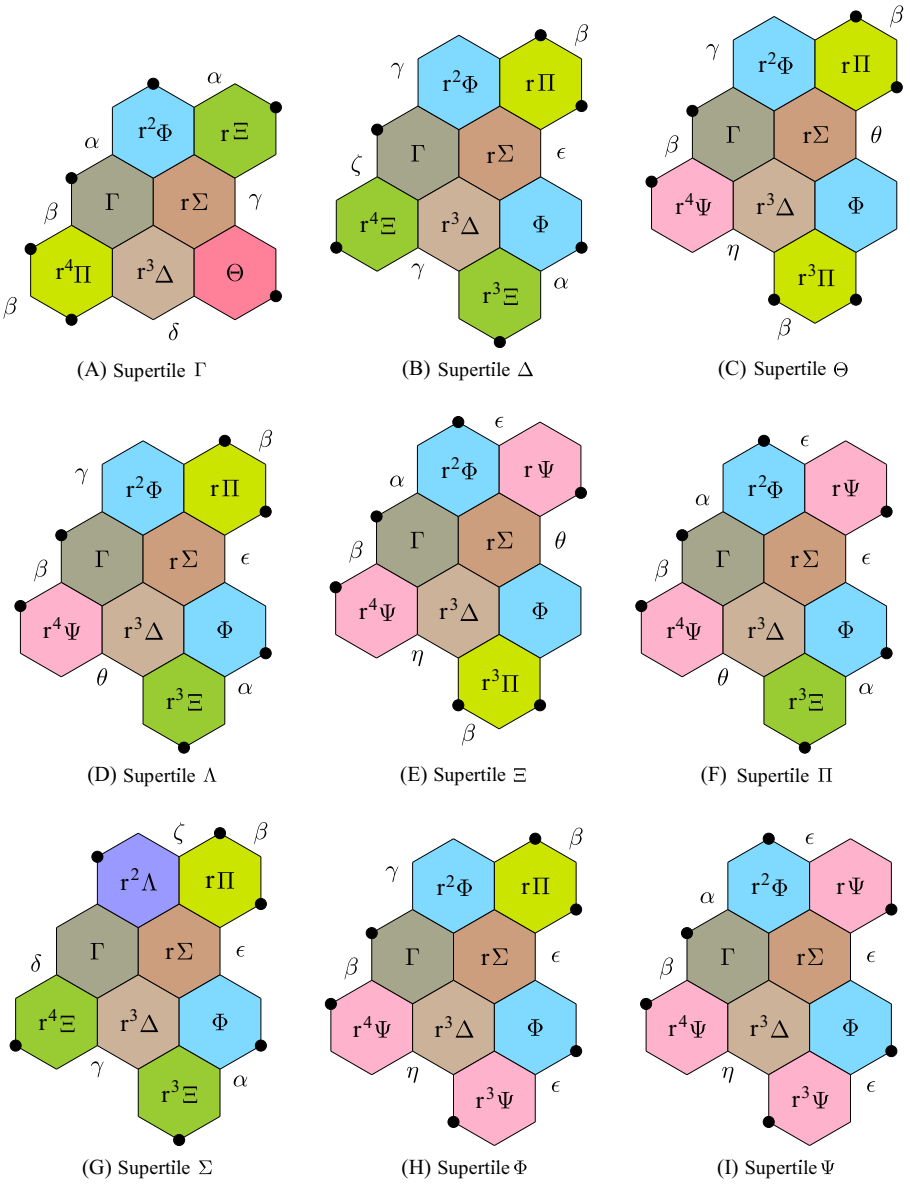

Fig. 4 Nine supertiles (adapted from [21, Figure 5.1]). Each is drawn in the reverse handedness of the corresponding marked hexagon of Fig. 3, preserving the handedness of the marked hexagons within it

Fortunately, the (co)boundary maps on Γ_{AP} commute with rotation, so instead of using 10×45 or 45×54 matrices, we can use 3×8 and 8×9 matrices with entries that are polynomials in r. See [18, Sec. 4] for a discussion of this procedure, and of working with one representation of the rotation group C_6 at a time. The boundary maps can be

Content courtesy of Springer Nature, terms of use apply. Rights reserved.

read off from Fig. 3. The boundary map ∂_1 on edges is given by the matrix

$$\begin{pmatrix} 1 & 0 & 0 & 0 & 1 & 0 & 0 & 0 \\ 0 & -r & 0 & 0 & -r & 0 & 1 & 1-r \\ -r^3 & r^4 & 1-r^5 & r^2-r^4 & 0 & r^4-r^5 & -r^5 & 0 \end{pmatrix}, \tag{1}$$

while the boundary map ∂_2 of faces is given by the matrix

$$\begin{pmatrix} r^3-r & -r^3 & 0 & -r^3 & r^3 & 0 & -r^3 & 0 & r^3 \\ r^2-r^4 & -r & -r+r^2-r^3 & r^2-r & r^2-r^3 & r^2 & -r & r^2-r & r^2 \\ r^5 & r-1 & -1 & -1 & 0 & 0 & r & -1 & 0 \\ 1 & 0 & 0 & 0 & 0 & 0 & -r^5 & 0 & 0 \\ 0 & r^5 & 0 & r^5 & -r & r^5-r & r^5 & r^5-r^3 & -r-r^3+r^5 \\ 0 & r^2 & 0 & 0 & 0 & 0 & -1 & 0 & 0 \\ 0 & 0 & -r^2 & r & -r^2 & r & 0 & 0 & 0 \\ 0 & 0 & r & 0 & r & 0 & 0 & r & r \end{pmatrix} \tag{2}$$

The matrices M_1^* and M_2^* for the substitution on edges and faces can similarly be read off from Fig. 4. We get

$$M_1^* = \begin{pmatrix} 0 & -r^5 & 0 & r^2 & 0 & -r^5 & 0 & 0 \\ -r^5 & 0 & r^2 & r & 0 & 0 & 0 & 0 \\ 0 & 0 & 0 & 0 & 0 & 0 & 0 & 0 \\ 0 & 0 & 0 & 0 & 0 & 0 & 0 & 0 \\ r^2 & r & r-r^5 & -r^4 & r+r^2-r^5 & r & r+r^2-r^4-r^5 & r+r^2-r^4-r^5 \\ 0 & 0 & 0 & 0 & 0 & 0 & 0 & 0 \\ 0 & 0 & r^2 & r^2-r^5 & 0 & r^2 & r^2 & 0 \\ r^3 & 0 & -1 & 0 & -1 & 0 & -1 & r^3 \end{pmatrix},$$

and

$$M_2^* = \begin{pmatrix} 1 & 1 & 1 & 1 & 1 & 1 & 1 & 1 & 1 \\ r^5 & r^5 & r^5 & r^5 & r^5 & r^5 & r^5 & r^5 & r^5 \\ 1 & 0 & 0 & 0 & 0 & 0 & 0 & 0 & 0 \\ 0 & 0 & 0 & 0 & 0 & 0 & r^2 & 0 & 0 \\ r & r^4+r^5 & 0 & r^5 & 0 & r^5 & r^4+r^5 & 0 & 0 \\ r^4 & r & r+r^5 & r & r^5 & 0 & r & r & 0 \\ r & r & r & r & r & r & r & r & r \\ r^2 & 1+r^2 & 1+r^2 & 1+r^2 & 1+r^2 & 1+r^2 & 1 & 1+r^2 & 1+r^2 \\ 0 & 0 & r^4 & r^4 & r+r^4 & r+r^4 & 0 & r^4+r^5 & r+r^4+r^5 \end{pmatrix}.$$

The matrices describing two rounds of substitution, taking unreflected meta-tiles to unreflected meta-tiles, are then $M_1^* M_1$ and $M_2^* M_2$, with the details as follows.

Content courtesy of Springer Nature, terms of use apply. Rights reserved.

As in [5, Sec. 2], we work with one representation of C_6 at a time. That is, we replace r with a power of ξ in (1) and (2) and compare kernels and images of ∂_1 and ∂_2 and eigenspaces of $M_1^* M_1$ and $M_2^* M_2$. Since we are computing cohomology rather than homology, we are acting by ∂_1 and ∂_2 on the right and our kernels and images will be sets of row vectors, not column vectors. Since $r^3\eta = -\eta$, the last column of ∂_1 and M_1^* and the last row of ∂_2 and M_1^* should be deleted when $r^3 \neq -1$, or in other words, when $r = 1, \xi^2$, or ξ^4. Since $r^2 p = p$ and $r^2 q = q$, the first two rows of ∂_1 should be deleted when $r^2 \neq 1$, that is, when $r = \xi, \xi^2, \xi^4$ or ξ^5. Since reflection turns r into r^{-1}, and since the inverse of a unit complex number is its complex conjugate, the matrices M_1 and M_2 in each representation are just the complex conjugates of the matrices M_1^* and M_2^*.

We summarize the calculations and results, one representation at a time.

- $r = 1$. When $r = 1$, we have 3 vertices, 7 edges and 9 faces. The matrix ∂_1 has rank 2, while ∂_2 has rank 5. Since $2+5 = 7$, this representation contributes nothing to $\check{H}^1$. Since $9-5 = 4$, this representation contributes $\mathbb{C}^4$ to $H^2(\Gamma_{\text{AP}}, \mathbb{C})$. Picking generators of this 4-dimensional space, we see how these generators transform under $M_2^* M_2$. The 4×4 matrix that describes this action has rank 2 and non-zero eigenvalues $(4 \pm \sqrt{15})^2$. This representation thus only contributes $\mathbb{C}^2$ to $\check{H}^2(\Omega, \mathbb{C})$. The generators of $\check{H}^2(\Omega, \mathbb{C})$ can in fact be represented by cochains that count Spectres and Mystics without distinguishing between the different kinds of collared Spectres.
- $r = \xi$. When $r = \xi$, we have one vertex, 8 edges and 9 faces. The rank of ∂_1 is 1 while that of ∂_2 is 5. This representation then contributes $\mathbb{C}^2$ to $H^1(\Gamma_{\text{AP}}, \mathbb{C})$ and $\mathbb{C}^4$ to $H^2(\Gamma_{\text{AP}}, \mathbb{C})$. Under substitution, the first cohomology transforms with eigenvalues $4 \pm \sqrt{15}$, while the second cohomology transforms with eigenvalues $4 \pm \sqrt{15}$ and 0 (the latter twice). That is, all of the first cohomology survives to the direct limit, contributing $\mathbb{C}^2$ to $\check{H}^1(\Omega, \mathbb{C})$, but only a $\mathbb{C}^2$ subspace of $H^2(\Gamma_{\text{AP}}, \mathbb{C})$ survives to the direct limit.
- $r = \xi^2$. When $r = \xi^2$, we have one vertex, 7 edges and 9 faces. The rank of ∂_1 is 1 and the rank of ∂_2 is 6, so we get no first cohomology and a contribution of $\mathbb{C}^3$ to $H^2(\Gamma_{\text{AP}}, \mathbb{C})$. However, substitution on the cokernel of ∂_2 involves a 3×3 matrix of rank 1, whose only non-zero eigenvalue is 1. Consequently, only a single copy of $\mathbb{C}$ survives the direct limit to contribute to $\check{H}^2(\Omega, \mathbb{C})$.
- $r = -1$. When $r = -1$, we have 3 vertices, 8 edges and 9 faces. The ranks of ∂_1 and ∂_2 are 3 and 5, respectively. This representation contributes nothing to $H^1(\Gamma_{\text{AP}}, \mathbb{C})$ and $\mathbb{C}^4$ to $H^2(\Gamma_{\text{AP}}, \mathbb{C})$. The 4×4 matrix describing substitution on this $\mathbb{C}^4$ has rank 2, with a double non-zero eigenvalue 1. The direct limit of $\mathbb{C}^4$ under substitution thus is $\mathbb{C}^2$.
- $r = \xi^4$. The calculations for $r = \xi^4$ are identical (up to complex conjugation) to those for $r = \xi^2$.
- $r = \xi^5$. The calculations for $r = \xi^5$ are identical (up to complex conjugation) to those for $r = \xi$. □

Remark 2 $H^2(\Gamma_{\text{AP}}, \mathbb{C}) = \mathbb{C}^{22}$ is much bigger than $\check{H}^2(\Omega, \mathbb{C}) = \mathbb{C}^{10}$. In every single representation, two of the eigenvalues of substitution on $H^2(\Gamma_{\text{AP}}, \mathbb{C})$ are zero. As a

Content courtesy of Springer Nature, terms of use apply. Rights reserved.

result, $2 \cdot 6 = 12$ copies of $\mathbb{C}$ fail to survive to the direct limit. This strongly suggests that our description of the substitutive structure of the Spectre tiling space is overly complicated. A different collaring scheme, or a different set of basic shapes that get substituted, would yield a different AP complex and could plausibly yield a simpler cohomology calculation. Since the publication of the original approach [21], alternate substitutive schemes have been proposed [22]. It will be interesting to see how much the calculations can be streamlined by using them. ◊

Remark 3 The decomposition of the chain and cochain complexes of Γ_{AP} is justified when working over $\mathbb{C}$, but not when computing the integral cohomology $\check{H}^*(\Omega, \mathbb{Z})$. To compute the integral cohomology, we must replace each entry of ∂_1, ∂_2, M_1 and M_2 with a 6×6 matrix (with adjustments for the rows and columns that refer to η, p and q), replacing the number 1 with the identity matrix and replacing r with the cyclic permutation matrix

$$\begin{pmatrix} 0 & 0 & 0 & 0 & 0 & 1 \\ 1 & 0 & 0 & 0 & 0 & 0 \\ 0 & 1 & 0 & 0 & 0 & 0 \\ 0 & 0 & 1 & 0 & 0 & 0 \\ 0 & 0 & 0 & 1 & 0 & 0 \\ 0 & 0 & 0 & 0 & 1 & 0 \end{pmatrix}.$$

Comparing the (left-)kernels and images of these matrices shows that $\check{H}^1(\Omega, \mathbb{Z}) = \mathbb{Z}^4$ and that $\check{H}^2(\Omega, \mathbb{Z}) = \mathbb{Z}^{10}$. ◊

We recall some facts about shape changes from [9]. Shape changes to a d-dimensional tiling are classified, up to MLD equivalence, by $\check{H}^1(\Omega, \mathbb{R}^d)$; see [9, Thm. 2.1]. Since $d = 2$, we use $\mathbb{C}$ in place of $\mathbb{R}^2$. For a substitution tiling, the contracting subspace of $\check{H}^1(\Omega, \mathbb{R}^d)$ under substitution parametrizes shape changes that are topological conjugacies [9, Thm. 2.2]. In our calculation of $\check{H}^1(\Omega, \mathbb{C})$, this is the eigenspace of substitution with eigenvalue $4 - \sqrt{15}$. With these facts in hand, we now analyze shape changes for the Spectre tilings.

Theorem 4 *Any shape change obtained by changing the values of a and b is the composition of a rescaling, a rotation, and a topological conjugacy.*

Proof Changing a and b preserves 6-fold rotational symmetry. This means that the shape class of each tiling lies in the portion of $\check{H}^1(\Omega, \mathbb{C})$ that comes from the fundamental representation $r = \xi$. It is easy to check that changes in the parameters a and b correspond to linearly independent elements of $\check{H}^1(\Omega, \mathbb{C})$, so *all* rotationally symmetric shape changes are MLD to changes in a and b.

The action of substitution on rotationally symmetric shape classes has an expanding eigenvalue $4+\sqrt{15}$ and a contracting eigenvalue $4-\sqrt{15}$. All shape classes must have a nonzero component in the direction of the expanding eigenvector, as this accounts for the asymptotic areas of supertiles, which scale by $(4 + \sqrt{15})^2$ under substitution. Therefore, the shape class for any Spectre tiling can be obtained from that of any other Spectre tiling by first multiplying a and b by a nonzero complex number z and then adding a multiple of the contracting eigenvector. The first move is the same as rescaling the tiling by $|z|$ and rotating by the argument of z. The second move is a topological conjugacy.

Content courtesy of Springer Nature, terms of use apply. Rights reserved.

Note that not all values of a and b yield actual tiles Tile(a, b). The boundary of Tile(a, b) is a sequence of edges with displacements a and ib times powers of ξ. In some cases, this traces a figure 8 instead of a simple closed curve. In such cases, we must work instead with larger clusters, equivalent to what is obtained by substituting Hats and Mystics several times. Under substitution, the direction of the shape class in $\check{H}^1(\Omega, \mathbb{C})$ approaches the eigenvector with eigenvalue $4 + \sqrt{15}$, yielding shapes whose boundaries *are* simple closed curves. The only cost of this is that we have to treat the n-supertiles, rather than the individual Hats and Turtles (or Mystics), as the basic units of our tiling. □

We next extend our analysis to shape changes that may not respect rotational symmetry.

Theorem 5 *Any tiling space homeomorphic to a space of Spectre tilings is topologically conjugate to a linear transformation applied to an arbitrarily chosen Spectre tiling space.*

Proof Every homeomorphism of tiling spaces with *finite local complexity* (FLC) is homotopic to the composition of a shape change and an MLD equivalence [13, Cor. 8.3]. This implies that any FLC tiling space that is homeomorphic to a specific FLC tiling space Ω is MLD to the result of a shape change applied to Ω. However, we have already identified all of the shape changes to the Spectre space. Those that preserve rotational symmetry are equivalent to varying a and b, or, equivalently, to a combination of a topological conjugacy and a rescaling and rotation.

Next, we consider shape changes from the $r = \xi^5$ representation that break rotational symmetry. Among these are linear transformations, such as shears, that do not commute with rotation. Also among these are the eigenspace of substitution with eigenvalue $4-\sqrt{15}$. Together, these span the $\mathbb{C}^2$ of $\check{H}^1(\Omega, \mathbb{C})$ that comes from $r = \xi^5$.

Put another way, the entire space of shape changes has real dimension 8. Four of these dimensions are linear transformations (two of which involve expansion and rotation, while the other two involve shears). The other four correspond to the 2 complex-dimensional eigenspace of substitution with eigenvalue $4-\sqrt{15}$, all of which induce topological conjugacies. □

The proofs of Theorems 4 and 5 are essentially the same as the proofs of analogous results about the Hat tilings [5]. Once we know that $\check{H}^1(\Omega, \mathbb{C})$ is as small as it could possibly be, the rest follows.

4 CASPr, the Friendly Spectre

In what follows, we work exclusively with the meta-tiles, the combinatorial hexagons from Fig. 3, and call such tilings Spectre tilings, too. In order to find a self-similar representative of this family of Spectre tilings, we first determine its edge vectors by solving an eigenvalue equation. Specifically, the square of the edge inflation, $M_1^* M_1$, must scale the edge vectors by a factor $\lambda = 4 + \sqrt{15}$. A solution of the eigenvector

Content courtesy of Springer Nature, terms of use apply. Rights reserved.

equation $M_1^* M_1 \boldsymbol{e} = \lambda \boldsymbol{e}$, with $\xi = \mathrm{e}^{2\pi\,\mathrm{i}/6}$ as before, is given by

$$\begin{aligned} e_\alpha &= 2\xi + (1-\xi)\lambda, \\ e_\beta &= 1 - 3\xi + \xi\lambda, \\ e_\gamma &= -2 + 4\xi + (2-\xi)\lambda, \\ e_\delta &= -9 + 3\xi + 3\lambda, \\ e_\varepsilon &= 1 - \xi + \lambda, \\ e_\zeta &= -1 - 4\xi + (1+\xi)\lambda, \\ e_\theta &= -1 + \xi + 2\lambda, \\ e_\eta &= 1 + 2\xi + \lambda. \end{aligned} \tag{3}$$

All edge vectors are elements of the $\mathbb{Z}$-module $\mathbb{Z}[\xi, \lambda] = \langle 1, \xi, \lambda, \lambda\xi \rangle_{\mathbb{Z}}$. The edge vectors span the edge module E, which is a submodule of $\mathbb{Z}[\xi, \lambda]$ of index 9.

Remark 6 Let us comment on the natural number-theoretic setting of our system. The $\mathbb{Z}$-module $\mathcal{O} = \mathbb{Z}[\xi, \lambda]$ with $\xi = \mathrm{e}^{2\pi\,\mathrm{i}/6}$ and $\lambda = 4 + \sqrt{15}$ is a ring, and as such a non-maximal order of the quartic number field $K = \mathbb{Q}(\sqrt{-3}, \sqrt{-5}\,)$, which (applying Hilbert's theorem) can also be written as $K = \mathbb{Q}(\alpha)$ with $\alpha = \sqrt{5}\,\mathrm{e}^{2\pi\,\mathrm{i}/12}$; see [25] for the main properties of K.

The maximal order of K is $\mathcal{O}_K = \langle 1, \alpha, \alpha^2/5, \alpha^3/5 \rangle_{\mathbb{Z}}$, which contains all algebraic integers from K, and $\mathcal{O}$ is a submodule of index 3. In fact, keeping track of the indices, one has

$$\mathrm{i}\sqrt{3}\,\mathcal{O}_K \overset{3}{\subset} \mathcal{O} \overset{3}{\subset} \mathcal{O}_K,$$

where $\mathcal{O}$ is not an ideal in $\mathcal{O}_K$, because $1 \in \mathcal{O}$. In particular, $\mathcal{O}$ is not Dedekind — for instance, $3\mathcal{O}_K$ is an ideal both in $\mathcal{O}_K$ and in $\mathcal{O}$, but it is not invertible as a fractional $\mathcal{O}$-ideal. Let us also remark that $\mathcal{O}$ and $\mathcal{O}_K$ have the same unit group, which is

$$\mathcal{O}^\times = \mathcal{O}_K^\times = \langle \xi \rangle \times \langle \lambda\xi \rangle \simeq C_6 \times C_\infty.$$

This makes working with $\mathcal{O}$ rather natural in our setting. In particular, important objects such as the return module will be invariant under the action of the unit group.

Since the field K has class number 2, not all ideals of $\mathcal{O}_K$ are principal, and neither are those of $\mathcal{O}$. Non-principal $\mathcal{O}$-ideals will appear in our context, where we then meet the special situation that they are still generated by two elements. This follows from [12, Thm. 2.3], because both $\mathcal{O}$ and $\mathcal{O}_K$ are Gorenstein rings, and no other ring lies between them. ♢

The self-similar tiles are now obtained by replacing the combinatorial edges of the 9 hexagon tiles from Fig. 3 by the geometric edges from (3), thereby producing the geometric (non-regular) hexagon tiles shown in Fig. 5. In the latter, we have drawn certain clusters of tiles together, because these tiles will always occur together in any legal tiling. By construction, this self-similar tiling is related by a shape change to the

Content courtesy of Springer Nature, terms of use apply. Rights reserved.

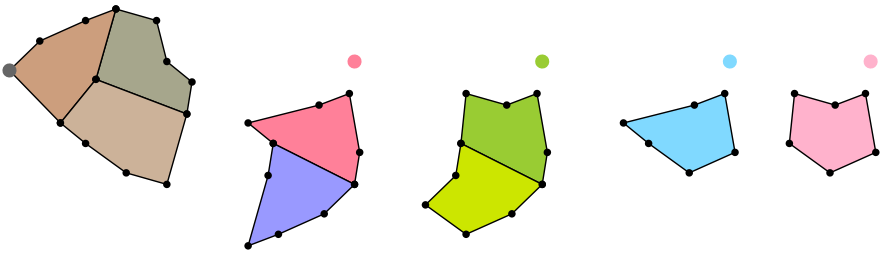

Fig. 5 Self-similar tiles of the CASPr tiling, with the edges from Eq. (3). From left to right are shown: the clusters $\Delta + \Gamma + \Sigma$, $\Lambda + \Theta$, and $\Pi + \Xi$, and the single tiles Φ and Ψ. Tiles which always occur together (the left three clusters) are drawn together. For each of these (clusters of) tiles, also its control point is shown (in 5 colors)

combinatorially equivalent tiling by regular hexagons, and hence is related by a shape change to the original Spectre tiling.

The inflation of the geometric tiles can now be read off from Fig. 4, again replacing the combinatorial edges by the geometric ones. The inflation of the tiles and clusters from Fig. 5 are shown in Fig. 6. We have drawn the (outer) supertile edges in different colors, depending on the type of the supertile edge. As one can see, if matching supertile edges are joined, each edge type always has the same environment on both sides, with the exception of the short β edge (red), which on one side can either have a Γ and a Ξ, or a Γ and a Ψ. However, the Ξ and the Ψ both touch the β superedge with their η edge (green), so that after one further inflation, also the β superedge always has the same environment on both sides. This proves that the inflation shown in Fig. 6 indeed forces the border, so that the simplified cohomology computation with uncollared tiles is justified. This is no surprise, of course, as the meta-tiles have been constructed with this goal in mind.

Let us explain one important subtlety that reflects the substitution structure from Sect. 3. Obviously, the tiles in Fig. 5 are not mirror-symmetric. We call them right-handed tiles. The outlines of the supertiles in Fig. 6 are left-handed, however. This is due to our use of a square root of the inflation described earlier: in one inflation step, we scale the tiling by $\sqrt{4+\sqrt{15}}$, reflect it (thus obtaining a tiling of left-handed supertiles), and replace each of these by a patch of right-handed tiles as shown in Fig. 6. Due to the reflection, this inflation is not a local subdivision of the scaled tiling, but its square is. A larger patch of tiles, generated by this inflation, is shown in Fig. 7, where one can see that, indeed, the tiles $\Delta + \Gamma + \Sigma$ (drawn in three different shades of brown) always occur together. The same holds for the pairs $\Xi + \Psi$ (green and yellow) and $\Lambda + \Theta$ (blue and red). We call this self-similar Spectre tiling the *friendly Spectre*, abbreviated as *CASPr* (for Cut-And-Symmetrically-Project).

Our method for taking the square root of the inflation $\sigma^*\sigma$ deserves a closer look. The inflation σ^* on the left-handed tiles is conjugate to σ via the horizontal reflection m, meaning $\sigma^* = m\sigma m$, so that $\sigma^*\sigma = (m\sigma)^2 = \widetilde{\sigma}^2$. In an analogous way, we can write the inflations on 1- and 2-cohomology as $M_1^* M_1 = \widetilde{M}_1^2$ and $M_2^* M_2 = \widetilde{M}_2^2$, respectively, in line with our approach above. Working with such square roots is often computationally simpler than working with M_i and M_i^* separately. We note that the

Content courtesy of Springer Nature, terms of use apply. Rights reserved.

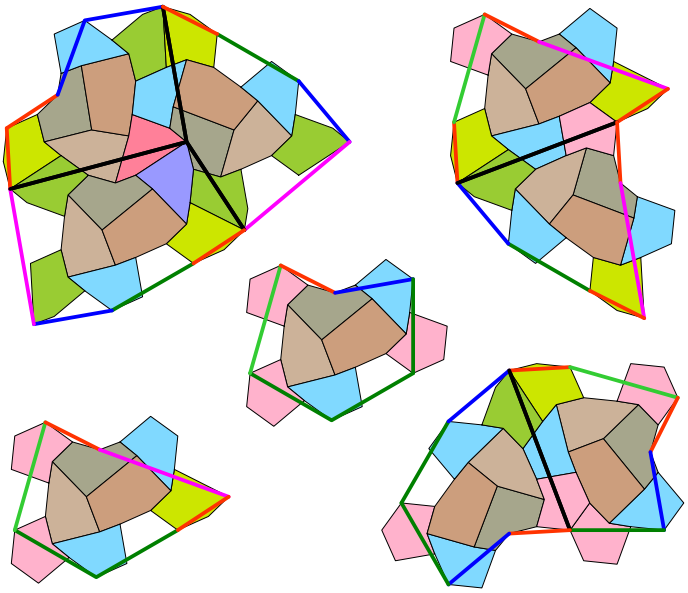

Fig. 6 Inflation of the tile clusters $\Delta + \Gamma + \Sigma$ (top left), $\Lambda + \Theta$ (top right), $\Pi + \Xi$ (bottom right), Ψ (centre), and Φ (bottom left). The (outer) supertile edges are drawn in color, as a function of edge type: blue for α, red for β, purple for γ, cyan for ε, and green for η. The remaining edge types only occur in the interior of these clusters

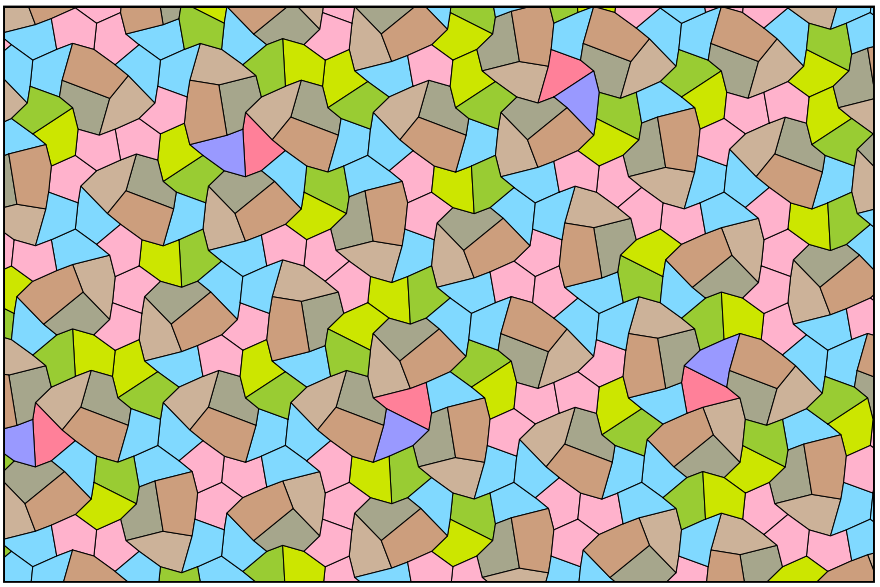

Fig. 7 Patch of a CASPr Tiling

Content courtesy of Springer Nature, terms of use apply. Rights reserved.

induced action of $\widetilde{M}_1$ on the edge module E leaves it invariant, whereas M_1 maps it to its mirror image, which is different. Conversely, $\widetilde{M}_1$ maps $\mathbb{Z}[\xi, \lambda]$ to a mirror image different from $\mathbb{Z}[\xi, \lambda]$, whereas M_1 leaves it invariant.

Another relevant module is the return module L, which is the $\mathbb{Z}$-span of all vectors translating a tile in a tiling to an equivalent tile in the same tiling. This is a submodule of the edge module E, given by the (right) kernel of ∂_1, projected to the edge module. The return module has index 9 in the edge module, and is invariant under $\widetilde{M}_1$, but not under M_1. Simple bases of E and L in terms of the (above chosen) standard basis of $\mathbb{Z}[\xi, \lambda]$ are given by

$$E = \langle (1,0,0,1), (0,-1,1,-1), (-1,-1,1,1), (0,1,2,1) \rangle_{\mathbb{Z}} \quad \text{and} \tag{4}$$

$$L = \langle (-1,-1,1,-2), (2,-1,1,1), (2,2,1,-2), (-2,1,2,2) \rangle_{\mathbb{Z}}. \tag{5}$$

In Fig. 5, we have added special reference points, so-called *control points*, to each tile or cluster of tiles. These have been chosen such that the set of control points of all tiles in a tiling lie in a single translation orbit of the return module, and such that the colored control point set is MLD with the tiling.

Remark 7 The return module L, viewed as a subset of $\mathbb{C}$, is a $\mathbb{Z}$-module with generators $1+\xi+2\lambda+5\lambda\xi$, $3\xi+6\lambda\xi$, $3\lambda+3\lambda\xi$, and $9\lambda\xi$. As such, it has index 81 in $\mathcal{O} = \mathbb{Z}[\xi, \lambda]$. Since $\mathbb{Z}[\xi, \lambda]L \subseteq L$, it is an *ideal* in $\mathcal{O}$, thus matching the rotation and inflation symmetry of the CASPr tiling. However, it is not principal, as mentioned before in Remark 6.

Via a standard lattice reduction algorithm, one finds $L = \langle g_1, g_2, g_3, g_4 \rangle_{\mathbb{Z}}$ with generators

$$\begin{aligned} g_1 &= -1 - \xi + \lambda - 2\lambda\xi, \\ g_2 &= 1 - 2\xi + 2\lambda - \lambda\xi = \xi g_1, \\ g_3 &= -2 + \xi + 2\lambda + 2\lambda\xi, \\ g_4 &= -1 - \xi - 2\lambda + 4\lambda\xi = \xi g_3. \end{aligned}$$

With this, one can identify L as the non-principal $\mathcal{O}$-ideal $L = (g_1, g_3) = (g_1) + (g_3)$. Alternatively, one can use generators in terms of α, where one choice is given by $L = \left(\frac{3}{5}\alpha^2 + 3\alpha + 6, \frac{3}{5}\alpha^3 + 3\alpha\right) = (3\xi + 3\alpha + 6, 3\alpha + 3\alpha\xi)$. We also note that L is an ideal both in $\mathcal{O}$ and in $\mathcal{O}_K$, and the given generators work for both variants. ◊

5 Embedding the Spectre

Equipped with the return module, we can now lift the Spectre tiling, or rather its set of control points, to a *cut-and-project scheme* (CPS) [7, Sec. 7.2]—provided the Spectre tiling has pure-point dynamical spectrum. The latter can be verified with the (generalized) overlap algorithm [3, 24] (which we have done prior to this step), or it can be proved in retrospect, after lifting the tiling (see below).

An element of $\mathbb{Z}[\xi, \lambda] \subset \mathbb{C}$ can be lifted to $\mathbb{C}^2$ by pairing it with its Galois conjugate (Minkowski embedding), where $\xi \mapsto \bar{\xi}$ and $\lambda \mapsto 8 - \lambda$. This induces a corresponding

Content courtesy of Springer Nature, terms of use apply. Rights reserved.

lifting of the return module $L \subset \mathbb{Z}[\xi, \lambda]$, and results in the CPS

$$\begin{array}{ccccc} \mathbb{C} & \xleftarrow{\pi} & \mathbb{C} \times \mathbb{C} & \xrightarrow{\pi_{\mathrm{int}}} & \mathbb{C} \\ \cup & & \cup & & \cup \text{ dense} \\ \pi(\mathcal{L}) & \xleftarrow{1:1} & \mathcal{L} & \longrightarrow & \pi_{\mathrm{int}}(\mathcal{L}) \\ \| & & & & \| \\ L & & \xrightarrow{\quad\star\quad} & & L^{\star} \end{array} \tag{6}$$

where $\mathcal{L} = \{(x, x^{\star}) : x \in L\}$ is the Minkowski embedding of the return module. By our choice, it agrees with the lattice generated by the lifted control points, and we have $L = \pi(\mathcal{L})$. Note that this simple connection between the return module and the embedding lattice only works for self-similar tilings. This is the reason for constructing a self-similar member of the Spectre tiling class. To continue, we shall also need the dual lattice $\mathcal{L}^*$ (note the different star symbol), as defined with respect to the standard inner product of $\mathbb{R}^4 \simeq \mathbb{C}^2$; see Remark 10 for more.

If we lift all control points of an inflation fixed point tiling, and project them to internal space, coloring them according to the tile or cluster type to which they belong, we obtain the picture shown in Fig. 8. Here, one can distinguish different subwindows, in which the projected control points of a given type are dense. Each subwindow has fractal boundaries with Hausdorff dimension

$$d_{\mathrm{H}} = \frac{\log(5+2\sqrt{6})}{\log(4+\sqrt{15})} \approx 1.110977, \tag{7}$$

as can be extracted from the orbit separation dimension of the CASPr tiling; see [4] for details. The fractal nature appears on different scales, but (unlike the window for the CAP tiling) the Hausdorff dimension seems to be the same everywhere along the boundary. This certainly deserves a closer analysis in the future.

Remark 8 A more detailed approach would proceed as follows. One starts with the inflation rule for the five effective prototiles from Fig. 5, and considers a fixed point of (a suitable even power of) the inflation. With respect to the control points, this defines the (translational) inflation displacement matrix, which has dimension 30 in this case (from the six distinct orientations of each of the five prototiles). This gives a fixed point equation for the 5-color Delone set of control points.

This equation can then be lifted via the $\star$-map to internal space, where (upon taking closures) it turns into a contractive iterated function system on $(\mathcal{K}\mathbb{C})^{30}$, where $\mathcal{K}\mathbb{C}$ is the space of non-empty compact subsets of $\mathbb{C}$ equipped with the Hausdorff distance; see [7, Sec. 7.1] for a one-dimensional example with all details of the construction. Its unique attractor consists of the 30 subwindows for the five types of control points, in six orientations each. When explicitly implementing this into an algebraic program, one can check [16] via the random tracing algorithm (known as the 'chaos game') that one indeed obtains the window system of Fig. 8. The justification of this step relies on Elton's ergodic theorem [10]; see [6] for further details. ◊

Content courtesy of Springer Nature, terms of use apply. Rights reserved.

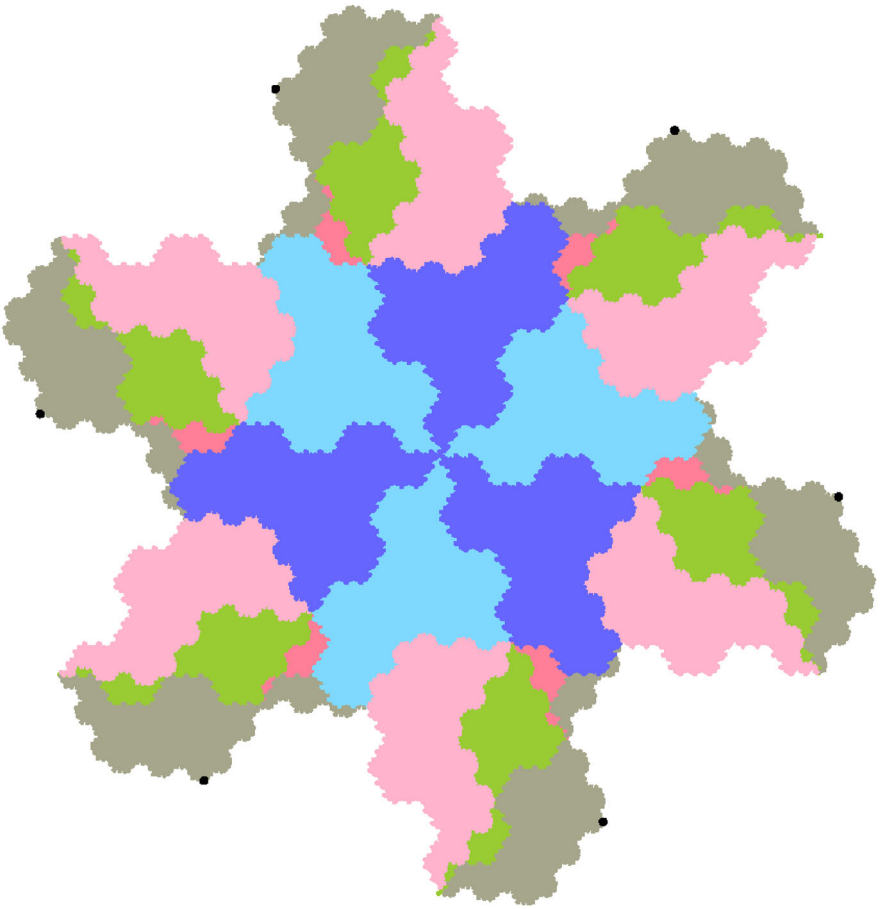

Fig. 8 Window system for the CPS of the CASPr tiling. The different subwindows are 5-colored according to the tile (cluster) type to which the control points belong. The light and dark blue subwindows in the middle belong to the same tile type; we have chosen different colors only to distinguish distinct orientations. The six black dots mark the corners of a regular hexagon that is a fundamental domain of a lattice. The window and its lattice translates form a tiling of the plane with a single 'fractile'

As already remarked at the beginning of this section, we have verified that the CASPr tiling has pure-point dynamical spectrum using the (generalized) overlap algorithm [3, 24]. As this is a computer-assisted proof, which is not easily repeated, we sketch here an alternative proof, which can be verified by hand, just as we did for the Hat tiling [5].

In order to verify that the Spectre tiling has pure-point spectrum, we employ the equivalence theorem between pure-point diffraction and dynamical spectrum [8, Thm. 7] and establish that the diffraction measure is pure point. This is clear for the covering model set by [7, Thm. 9.4]. Since the diffraction measure of a point set is not affected by a change of density 0 to the point set, compare [7, Sec. 8.8], it suffices to show that the point density of the covering model set determined from the CPS agrees

Content courtesy of Springer Nature, terms of use apply. Rights reserved.

with the true control point density. This then means that the windows for the different tile types have no overlap of positive measure. The control point density from the CPS, by the standard uniform distribution property of the $\star$-image in internal space, see [17] and [7, Prop. 9.9], is given by the area A of the window, divided by the volume V of a unit cell of $\mathcal{L}$. For the unit cell volume, we obtain

$$V \;=\; \tfrac{3}{4}\,\det\begin{pmatrix} 1 & \lambda \\ 1 & 8-\lambda \end{pmatrix}^2 \cdot 81 \;=\; 3645,$$

where 81 is the index of $\mathcal{L}$ in the lift of $\mathbb{Z}[\xi, \lambda]$. To determine the area A of the window, one can convince oneself (via Fig. 8) that the window is a fundamental domain of a triangular lattice, with a generating vector $d = 31 + 4(\xi - \lambda) - \lambda\xi$, which gives a window area of

$$A \;=\; \tfrac{\sqrt{3}}{2}\,|d|^2 \;=\; \tfrac{135\sqrt{3}}{2}\,(8-\lambda).$$

The control point density from the CPS is then given by

$$\rho_1 \;=\; \tfrac{A}{V} \;=\; \tfrac{(8-\lambda)\sqrt{3}}{54}.$$

This density ρ_1 now has to be compared to the true control point density, which can be computed as follows. The right Perron–Frobenius eigenvector of the tile inflation matrix contains the relative frequences of the different tile types. If we normalize the sum of these frequences to 1, we obtain the vector

$$\begin{aligned} \boldsymbol{f} \;=\; (&8-\lambda,\, 8-\lambda,\, 63-8\lambda,\, 63-8\lambda,\, 15\lambda-118,\\ &15\lambda-118,\, 8-\lambda,\, 14\lambda-110,\, 197-25\lambda). \end{aligned}$$

We see that there is a triple and two pairs of tiles with the same frequency. These form the tile clusters which always occur together. Taking the scalar product of the frequency vector and the vector of tile areas computed with the self-similar tile edges, we obtain the average tile area, which evaluates to $90\sqrt{3}$. The tile density then is $\sqrt{3}/270$. However, we now have to remember that we were counting only one control point per tile cluster, so that we must multiply this density with the sum of the *distinct* frequencies in the frequency vector $\boldsymbol{f}$. This then gives a total control point density of

$$\rho_2 \;=\; \tfrac{5(8-\lambda)\sqrt{3}}{270} \;=\; \tfrac{(8-\lambda)\sqrt{3}}{54} \;=\; \rho_1.$$

Hence, the two control point densities agree, which proves the following result, and corroborates the result of the overlap algorithm.

Theorem 9 *The control points of the CASPr tiling comprise a full-density subset of the 5-color regular model set defined by the window system from Fig. 8. They are dynamically defined Rauzy fractals, whose boundaries have the Hausdorff dimension from Eq. (7).*

Content courtesy of Springer Nature, terms of use apply. Rights reserved.

As such, the CASPr tiling has pure-point diffraction, with the Fourier module

$$L^{\circledast} = \pi_{\mathrm{int}}(\mathcal{L}^*).$$

The latter agrees with the dynamical pure-point spectrum of the CASPr tiling, when viewed as a dynamical system under the translation action of $\mathbb{R}^2$*. This system is strictly ergodic and has continuously representable eigenfunctions.* □

Remark 10 Let us expand on the role of $L^{\circledast}$ within the number field $K = \mathbb{Q}(\alpha)$ from Remark 6. Observe first that the dual module of the non-maximal order $\mathcal{O} = \mathbb{Z}[\xi, \lambda]$ is

$$\mathbb{Z}[\xi, \lambda]^* = \tfrac{\mathrm{i}\sqrt{5}}{15}\, \mathbb{Z}[\xi, \lambda],$$

where $\mathbb{Z}[\xi, \lambda]$ is a submodule of its dual of index 45^2. The dual of a $\mathbb{Z}$-module $M \subset K$ is defined as $M^* = \{y \in K : x.y + (x.y)' \in \mathbb{Z} \text{ for all } x \in M\}$, with $x.y := \frac{1}{2}(\bar{x}y + x\bar{y})$. Here, $(.)'$ is the non-trivial algebraic conjugation in $\mathbb{Q}(\sqrt{15}\,)$, given by $\sqrt{15} \mapsto -\sqrt{15}$. Note that $x.y$ lies in this field for all $x, y \in K$, because $x.y = \mathrm{Re}(\bar{x}y) \in K \cap \mathbb{R} = \mathbb{Q}(\sqrt{15}\,)$, which is the maximal real subfield of K. This form is $\mathbb{R}$-linear and designed to match the duality notion in Euclidean 4-space, relative to the standard inner product, as this fits best to the use of the Fourier transform.

Further, the dual of the maximal order is $\mathcal{O}_K^* = \frac{\sqrt{15}}{15}\mathcal{O}_K$. In fact, one has

$$L \overset{9^2}{\subset} \mathcal{O} \overset{3}{\subset} \mathcal{O}_K \overset{15^2}{\subset} \mathcal{O}_K^* = \tfrac{\sqrt{15}}{15}\mathcal{O}_K \overset{3}{\subset} \mathcal{O}^* = \tfrac{\mathrm{i}\sqrt{5}}{15}\mathcal{O} \overset{9^2}{\subset} L^*,$$

again keeping track of the indices, and all matches up so that $L^{\circledast} = L^*$ in this sense, and so that $L^{\circledast} = \pi(\mathcal{L}^*)$, where $\mathcal{L}^*$ is the (standard) dual of the lattice $\mathcal{L}$ in $\mathbb{C}^2 \simeq \mathbb{R}^4$. The justification of this computation comes from the dual CPS, which (in our case) can be combined with the original CPS because $\mathbb{C}$ and $\mathbb{C}^2$ are self-dual as locally compact Abelian groups.

We still need a good way to express L^*. In Remark 7, we identified the return module as the non-principal ideal (g_1, g_3) of $\mathbb{Z}[\xi, \lambda]$. Now, if $\mathrm{N}(z)$ denotes the field norm of $z \in K$, which is $\mathrm{N}(z) = z\bar{z}z'\bar{z}'$, one can verify that the dual of a principal $\mathcal{O}$-ideal is

$$(z)^* = \tfrac{1}{\bar{z}}\mathbb{Z}[\xi, \lambda]^* = \tfrac{zz'\bar{z}'}{\mathrm{N}(z)}\, \tfrac{\mathrm{i}\sqrt{5}}{15}\, \mathbb{Z}[\xi, \lambda].$$

Then, with $L = (g_1) + (g_3)$ from Remark 7, some explicit computation leads to

$$L^{\circledast} = L^* = (g_1)^* \cap (g_3)^* = \tfrac{\mathrm{i}\sqrt{5}}{135}\, L.$$

This shows that $L^{\circledast}$ is a non-principal, fractional ideal, whose generators can now be given as (fractional) multiples of the generators of L from Remark 7, which is one of the simplest ways to pin down the Fourier module. ◊

Content courtesy of Springer Nature, terms of use apply. Rights reserved.

6 The Spectre is MLD to a Re-projected Model Set

Consider what happens when we take the same 4-dimensional total space as for the CASPr tiling, the same lattice, and the same acceptance strip, only we vary the projection from $\mathbb{R}^4$ to $\mathbb{R}^2$. Varying the projection moves each point in $\mathbb{R}^2$ by a linear function of its corresponding coordinates in perpendicular space. This results in a topological conjugacy, since the perpendicular coordinates are 'weakly pattern equivariant', but not an MLD equivalence, insofar as the perpendicular coordinates cannot be determined exactly from the local pattern; we refer to [15, Secs. 3.6 and 3.7] for a discussion of reprojections and pattern equivariance.

In particular, the tilings obtained by varying the projection in the CASPr tiling form a (real) 4-dimensional family that is topologically conjugate to CASPr, but not MLD. However, we have already determined that, up to MLD equivalence, the set of tilings that are topologically conjugate to CASPr is a connected 4-dimensional family. The upshot is that all tilings that are topologically conjugate to the CASPr are MLD to reprojections of the CASPr control points. In particular, all of the tilings that are obtained by varying the (complex) ratio a/b, including the original Spectre tiling, are MLD to reprojections of CASPr.

Let us illustrate this with two different reprojections. The first and simpler one relies on the CASPr tiling being combinatorially equivalent to a tiling of regular hexagons (compare Fig. 3), which have vertices in a simple hexagonal lattice. We can therefore index the vertices of a CASPr tiling also with vectors from that lattice. The correspondence between the 4-dimensional CASPr indices and the new 2-dimensional hexagonal indices of the CASPr vertices defines a linear map from the CASPr return module L to the hexagonal lattice. If we choose the right orientation and scale for the latter, this linear map is the reprojection of the CASPr control points we are looking for. The right scale is easily obtained by requiring that the regular hexagons are in area equal to the average area of the CASPr tiles, which is known. In the left panel of Fig. 9, we show a patch of a CASPr tiling reprojected in this way, along with its reprojected control points. The CASPr tiles are considerably distorted under reprojection, but clearly recognizable. For comparison, on the right hand side of the figure, we show the corresponding regular hexagon tiling, which is obviously MLD to the reprojected CASPr tiling: The control points of the two tilings agree exactly.

Instead of regular hexagons, we can also use the meta-tiles of the Hat–Turtle tiling (see [21, Fig. 4.1]). These meta-tiles also form a combinatorial hexagon tiling, whose tile edges take values in another hexagon lattice, and we can index the CASPr vertices also with respect to that hexagon lattice. This leads to yet another reprojection map. The reprojected CASPr tiling it produces is MLD to a corresponding meta-tile tiling. Such a pair is shown in Fig. 10. The reprojected CASPr tiles, shown on the left, are now quite close to the true CASPr tiles. Again, the two patches are MLD to each other, with exactly the same control points.

Corollary 11 *The Spectre tiling is MLD with a* 5*-color Meyer set that is a re-projection of the points from the cut-and-project description of the CASPr tiling from Theorem 9. In particular, the translation dynamical system of the Spectre tiling has the same pure-*

Content courtesy of Springer Nature, terms of use apply. Rights reserved.

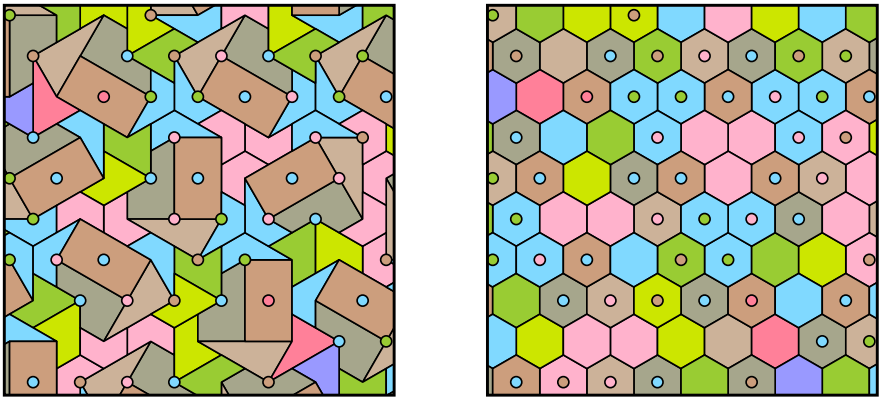

Fig. 9 Patch of a reprojected CASPr tiling (left) and the corresponding patch of a regular hexagon tiling which is MLD to it (right). The two patches have exactly the same control points. Note that, like for the CASPr, the control points are a bit away from their tiles

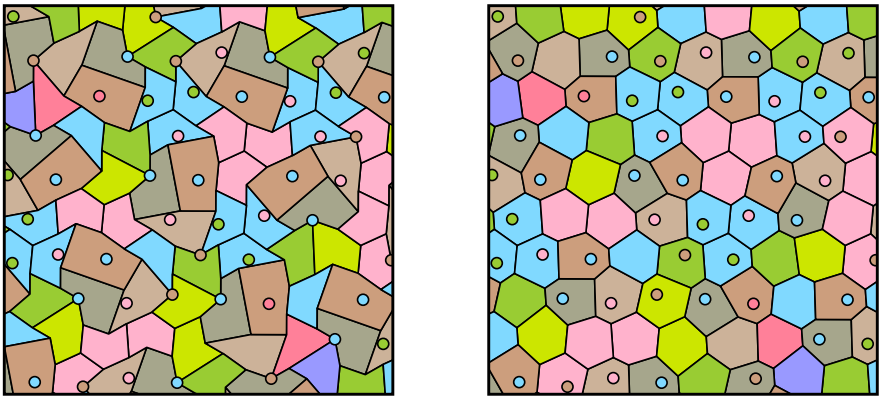

Fig. 10 Patch of a reprojected CASPr tiling (left) and the corresponding patch of a meta-tile tiling which is MLD to it (right). The two patches have exactly the same control points

point spectrum with continuously representable eigenfunctions. All this holds, in fact, for all *Spectre-like tilings.* □

It is worth noting what changes and what does not change under reprojection. As an abstract dynamical system, the tiling space does not change. This implies that the dynamical spectrum, namely the action of translation on $L^2(\Omega)$, does not change. This in turn implies that the diffraction pattern generated by the control points remains pure point, with the exact same Bragg peak locations.

However, the intensity of the Bragg peaks can vary. As we continuously change CASPr into the Spectre tiling, adjusting the positions of the control points, some Bragg peaks become more intense while others fade. To the naked eye, the two diffraction patterns show rather different features [6], even though they are supported on the same

Content courtesy of Springer Nature, terms of use apply. Rights reserved.

points. Various further details, including the deformation maps and the diffraction images, will be given there.

Acknowledgements It is our pleasure to thank Markus Kirschmer for helpful discussions on the number-theoretic structure. We thank two anonymous referees for their thoughtful comments, which helped us to improve the presentation. This work was supported by the German Research Council (Deutsche Forschungsgemeinschaft, DFG) under SFB-TRR 358/1 (2023) – 491392403 and by the National Science Foundation under grant DMS-2113468.

Funding Open Access funding enabled and organized by Projekt DEAL.

Data Availability No data were used, created or processed during this work.

Open Access This article is licensed under a Creative Commons Attribution 4.0 International License, which permits use, sharing, adaptation, distribution and reproduction in any medium or format, as long as you give appropriate credit to the original author(s) and the source, provide a link to the Creative Commons licence, and indicate if changes were made. The images or other third party material in this article are included in the article's Creative Commons licence, unless indicated otherwise in a credit line to the material. If material is not included in the article's Creative Commons licence and your intended use is not permitted by statutory regulation or exceeds the permitted use, you will need to obtain permission directly from the copyright holder. To view a copy of this licence, visit http://creativecommons.org/licenses/by/4.0/.

References

1. Akiyama, S., Araki, Y.: An alternative proof for an aperiodic monotile. Discrete Comput. Geom. (2025) (**in press**); arXiv:2307.12322
2. Anderson, J.E., Putnam, I.F.: Topological invariants for substitution tilings and their associated C^*-algebras. Ergod. Theory Dyn. Syst. **18**, 509–537 (1998)
3. Akiyama, S., Lee, J.-Y.: Algorithm for determining pure pointedness of self-affine tilings. Adv. Math. **226**, 2855–2883 (2011). arXiv:1003.2898
4. Baake, M., Gähler, F., Gohlke, P.: Orbit separation dimension as complexity measure for primitive inflation tilings. Ergod. Theory Dyn. Syst. (2025) (**in press**); arXiv:2311.03541
5. Baake, M., Gähler, F., Sadun, L.: Dynamics and topology of the Hat family of tilings. Israel J. Math. (2025) (**in press**); arXiv:2305.05639
6. Baake, M., Gähler, F., Mazáč, J., Mitchell, A.: Diffraction of the Hat and Spectre tilings and some of their relatives. J. Math. Phys. (2025) (**in press**); arXiv:2502.03268
7. Baake, M., Grimm, U.: Aperiodic Order. Vol. 1: A Mathematical Invitation. Cambridge University Press, Cambridge (2013)
8. Baake, M., Lenz, D.: Dynamical systems on translation bounded measures: pure point dynamical and diffraction spectra. Ergod. Theory Dyn. Syst. **24**, 1867–1893 (2004). arXiv:math.DS/0302061
9. Clark, A., Sadun, L.: When shape matters. Ergod. Theory Dyn. Syst. **26**, 69–86 (2006). arXiv:math.DS/0306214
10. Elton, J.H.: An ergodic theorem for iterated maps. Ergod. Theory Dyn. Syst. **7**, 481–488 (1987)
11. Frank, N.P., Sadun, L.: Fusion: a general framework for hierarchical tilings of $\mathbb{R}^d$. Geom. Dedic. **171**, 149–186 (2014). arXiv:1101.4930
12. Greither, C.: On the two generator problem for the ideals of a one-dimensional ring. J. Pure Appl. Alg. **24**, 265–276 (1982)
13. Julien, A., Sadun, L.: Tiling deformations, cohomology, and orbit equivalence of tiling spaces. Ann. H. Poincaré **19**, 3053–3088 (2018). arXiv:1506.02694
14. Kellendonk, J.: Noncommutative geometry of tilings and gap labelling. Rev. Math. Phys. **7**, 1133–1180 (1995). arXiv:cond-mat/9403065
15. Kellendonk, J., Sadun, L.: Conjugacies of model sets. Discrete Cont. Dyn. Syst. A **37**, 3805–3830 (2017). arXiv:1406.3851
16. Mazáč, J.: Fractal and Statistical Phenomena in Aperiodic Order, PhD thesis, Bielefeld University (2025)

Content courtesy of Springer Nature, terms of use apply. Rights reserved.

17. Moody, R.V.: Uniform distribution in model sets. Can. Math. Bull. **45**, 123–130 (2002)
18. Ormes, N., Radin, C., Sadun, L.: A homeomorphism invariant for substitution tiling spaces. Geom. Dedic. **90**, 153–182 (2002). arXiv:math.DS/0008171
19. Sadun, L.: Topology of Tiling Spaces. American Mathematical Society, Providence (2008)
20. Smith, D., Myers, J.S., Kaplan, C.S., Goodman-Strauss, C.: An aperiodic monotile. Combin. Theory **4**(6), 1–90 (2024). arXiv:2303.10798
21. Smith, D., Myers, J.S., Kaplan, C.S., Goodman-Strauss, C.: A chiral aperiodic monotile. Combin. Theory **4**(13), 1–25 (2024). arXiv:2305.17743
22. Smith,J.: Turtles, hats and spectres: aperiodic structures on a rhombic tiling, preprint (2024); arXiv:2403.01911
23. Socolar, J.E.S., Taylor, J.M.: An aperiodic hexagonal tile. J. Comb. Theory A **118**, 2207–2231 (2011). arXiv:1003.4279
24. Solomyak, B.: Dynamics of self-similar tilings. Ergod. Theory Dyn. Syst. **17**, 695–738 (1997) and Ergod. Theory Dyn. Syst. **19** (1999) 1685 (erratum)
25. The LMFDB Collaboration, The L-functions and Modular Forms Database (2024), entry 4.0.3600.3, available at https://www.lmfdb.org/NumberField/4.0.3600.3

Publisher's Note Springer Nature remains neutral with regard to jurisdictional claims in published maps and institutional affiliations.

Content courtesy of Springer Nature, terms of use apply. Rights reserved.

Terms and Conditions

Springer Nature journal content, brought to you courtesy of Springer Nature Customer Service Center GmbH ("Springer Nature").

Springer Nature supports a reasonable amount of sharing of research papers by authors, subscribers and authorised users ("Users"), for small-scale personal, non-commercial use provided that all copyright, trade and service marks and other proprietary notices are maintained. By accessing, sharing, receiving or otherwise using the Springer Nature journal content you agree to these terms of use ("Terms"). For these purposes, Springer Nature considers academic use (by researchers and students) to be non-commercial.

These Terms are supplementary and will apply in addition to any applicable website terms and conditions, a relevant site licence or a personal subscription. These Terms will prevail over any conflict or ambiguity with regards to the relevant terms, a site licence or a personal subscription (to the extent of the conflict or ambiguity only). For Creative Commons-licensed articles, the terms of the Creative Commons license used will apply.

We collect and use personal data to provide access to the Springer Nature journal content. We may also use these personal data internally within ResearchGate and Springer Nature and as agreed share it, in an anonymised way, for purposes of tracking, analysis and reporting. We will not otherwise disclose your personal data outside the ResearchGate or the Springer Nature group of companies unless we have your permission as detailed in the Privacy Policy.

While Users may use the Springer Nature journal content for small scale, personal non-commercial use, it is important to note that Users may not:

1. use such content for the purpose of providing other users with access on a regular or large scale basis or as a means to circumvent access control;
2. use such content where to do so would be considered a criminal or statutory offence in any jurisdiction, or gives rise to civil liability, or is otherwise unlawful;
3. falsely or misleadingly imply or suggest endorsement, approval , sponsorship, or association unless explicitly agreed to by Springer Nature in writing;
4. use bots or other automated methods to access the content or redirect messages
5. override any security feature or exclusionary protocol; or
6. share the content in order to create substitute for Springer Nature products or services or a systematic database of Springer Nature journal content.

In line with the restriction against commercial use, Springer Nature does not permit the creation of a product or service that creates revenue, royalties, rent or income from our content or its inclusion as part of a paid for service or for other commercial gain. Springer Nature journal content cannot be used for inter-library loans and librarians may not upload Springer Nature journal content on a large scale into their, or any other, institutional repository.

These terms of use are reviewed regularly and may be amended at any time. Springer Nature is not obligated to publish any information or content on this website and may remove it or features or functionality at our sole discretion, at any time with or without notice. Springer Nature may revoke this licence to you at any time and remove access to any copies of the Springer Nature journal content which have been saved.

To the fullest extent permitted by law, Springer Nature makes no warranties, representations or guarantees to Users, either express or implied with respect to the Springer nature journal content and all parties disclaim and waive any implied warranties or warranties imposed by law, including merchantability or fitness for any particular purpose.

Please note that these rights do not automatically extend to content, data or other material published by Springer Nature that may be licensed from third parties.

If you would like to use or distribute our Springer Nature journal content to a wider audience or on a regular basis or in any other manner not expressly permitted by these Terms, please contact Springer Nature at

onlineservice@springernature.com